

Instrument Science Report NICMOS 2009 - 008

NICMOS Breathing and Focus Field Variations

Tommy Wiklind & Deepashri Thatte

June 30 2009

ABSTRACT

The focus of the NICMOS cameras is monitored on a regular basis. In order to achieve consistency in the focus determination, several effects have to be taken into consideration. The main ones affecting NICMOS are: (1) thermally induced movement of the secondary mirror (a.k.a. breathing), and (2) a curved focal plane for all three cameras. The latter is known as NICMOS Focus Field Variation and affects both the measurement of the focus and gives a position dependent Point Spread Function. In this Instrument Science Report we discuss the breathing corrections in the context of the NICMOS Focus Monitoring Program, and re-measure the Focus Field Variations.

Introduction

The NICMOS cameras were originally supposed to share a common focus, whose position can be adjusted with the Pupil Alignment Mechanism (PAM). The PAM's main part consists of an adjustable mirror, moving ± 10 mm about its mechanical zero position, allowing a fine-tuning of the focus. Any change introduced in the optical path to the HST secondary mirror (SM) can then be compensated for by moving the PAM. However, the deformation of the

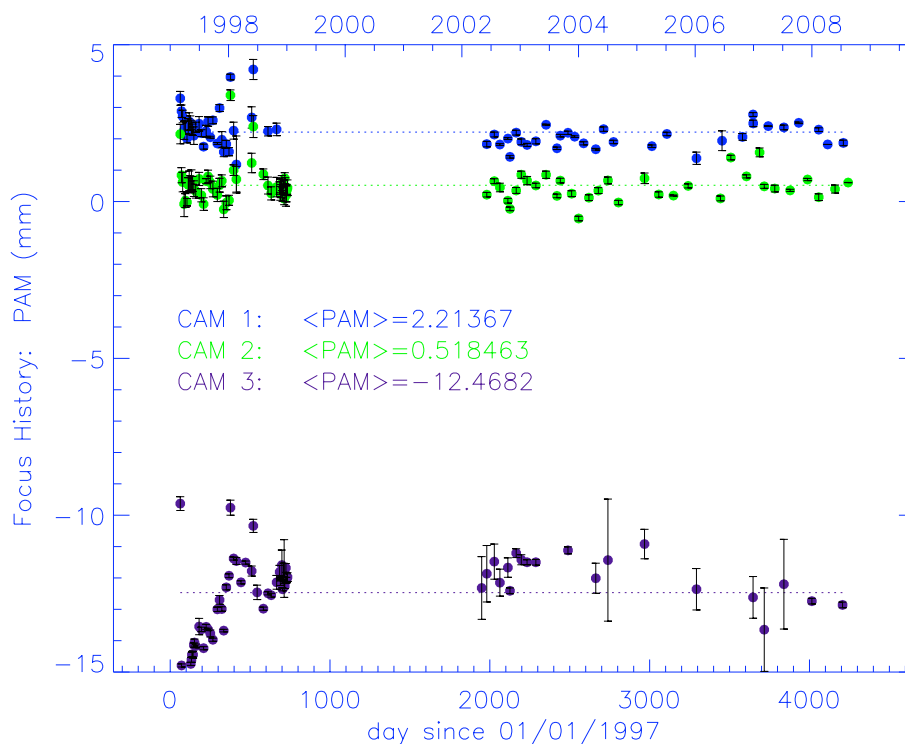


Fig. 1.— *The results from the NICMOS focus monitoring program during the period 1997–1999 and following SM3b in March 2002. The average best PAM position for the three cameras are listed in the figure.*

NICMOS dewar, occurring shortly after the installation of NICMOS in 1997, caused a large mechanical distortion, resulting in the loss of a common focus for the three cameras. The NIC3 camera suffered the largest deformation, being pushed out of range for the available PAM movement. Best focus for NIC3 is currently beyond the maximum range setting of the PAM at -12.5 mm. The initial displacement of the NIC3 focus was -17 mm, but since the dewar continued to deform during cycle 7, the actual NIC3 offset improved with time. The current location of the NIC3 focus has been relatively stable for several years. The best focus for NIC1 and NIC2 is achieved with a PAM position of $+2$ mm and $+0.2$ mm, respectively.

The NICMOS focus has been monitored by the NICMOS Team at STScI on a regular basis (see Figure 1). Since the installation of the NICMOS Cooling System (NCS) in March 2002, monitoring has been done on a monthly or bimonthly schedule for NIC1 and NIC2, and less frequently for NIC3.

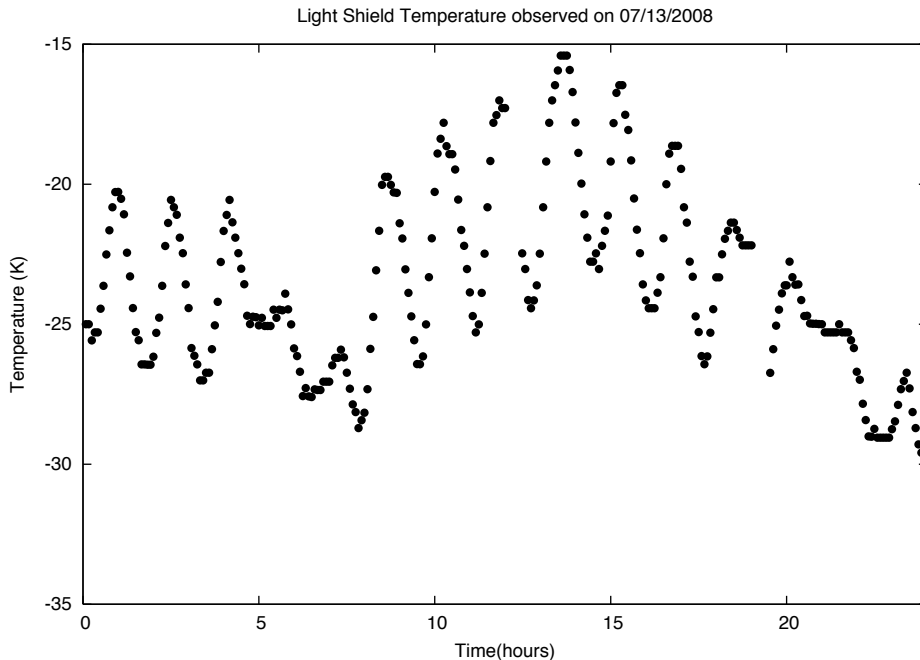


Fig. 2.— Variation of the HST Light Shield temperature during 24 hours.

While there are occasional excursions in values of the best PAM position, the NIC1 and NIC2 cameras have shown approximately constant focus during the last seven years (Figure 1). Since NICMOS is operating at wavelengths longer than $\sim 1 \mu\text{m}$ its image quality is less sensitive to small focus changes compared to instruments operating at optical/UV wavelengths. It is nevertheless desirable to be able to characterize the NICMOS focus and its variability as precisely as possible. This allows detecting long term changes in the deformation of the NICMOS dewar and its optical components and a better understanding and characterization of the point spread function (PSF).

Apart from internal causes, the NICMOS focus is also affected by changes in the optical path length in the HST telescope assembly. These changes can be seen on an orbital, annual and longer time scales. On a yearly and shorter time scale, the changes are mainly the result of thermal variations in the telescope structure. Focus changes over longer time scales are due to an overall shrinking of the telescope assembly, caused by the release of gases from the HST structure (Di Nino et al. 2008). The latter effect has caused a decrease in the optical path by $\sim 13 \mu\text{m}$ over a period of six years. The secondary mirror has been moved back three times over this period to compensate for the change in the optical path length. The change in the location of the secondary mirror (ΔSM) is measured in microns and translates to changes in the NICMOS PAM space (ΔPAM) as

$$\Delta\text{PAM} = 0.11 \times G_i \times \Delta\text{SM}_{\mu\text{m}} \text{ mm}, \quad (1)$$

where $G_i = 1.171, 1.212$ and 1.083 for NIC1, NIC2 and NIC3, respectively (Burrows & Krist, 1997). In addition to this approximately monotonic change in focus, the optical path length varies over orbital time scales due to thermal changes. This effect is known as 'breathing' and can change the optical path length by a few microns on time scales of the HST orbit. This transforms to a NICMOS PAM shift of a few tenths of a millimeter. Since the HST breathing is caused by temperature variations, it can be modelled using temperature sensors in the light shield surrounding the secondary mirror:

$$\Delta\text{SM} = 0.7 (T_{LS4} - \langle T_{LS4} \rangle) \mu\text{m}, \quad (2)$$

where T_{LS4} is the light shield temperature and $\langle T_{LS4} \rangle$ is the time average of the mean light shield temperature over the preceding orbit. A focus model including both the monotonic shrinking of the HST telescope assembly and thermal effects is presented in Di Nino et al. (2008).

Despite the relatively large change in the optical path length since 2002, there is little evidence in the NICMOS focus monitoring data of a corresponding change in the focus for either of the three cameras. The latest focus correction of the secondary mirror involved a change of $5.34 \mu\text{m}$ in July 2006. This corresponds to 0.7 mm in PAM space and should have been detectable in the regular NICMOS focus monitoring data. This is, however, not the case. It is possible that such a change is masked by the orbital breathing and the curvature of the focus over the face of the detectors.

In this Instrument Report we revisit the breathing corrections for NICMOS and re-measure the focus field variations (FFV) in order to improve the precision with which we can determine the focus and test for secular changes in the focus and the curvature of the focal plane. A similar study was done when NICMOS was installed in HST in 1997 (Suchkov & Galas 1998).

Camera	$a_x \times 10^3$	$a_y \times 10^3$	$a_{xx} \times 10^5$	$a_{yy} \times 10^5$	$a_{xy} \times 10^5$
NIC1	-2.869 ± 1.529	1.383 ± 0.542	1.199 ± 0.416	0.229 ± 0.145	0.068 ± 0.227
NIC2	-1.304 ± 0.211	2.819 ± 0.168	0.397 ± 0.056	0.605 ± 0.061	0.614 ± 0.079
NIC3	-3.682 ± 0.159	-6.578 ± 0.120	1.580 ± 0.0166	1.710 ± 0.039	-0.055 ± 0.062

Table 1: *Coefficients of the FFV fit from Suchkov & Galas (1997).*

NICMOS Focus Effects

Breathing

The effect of breathing on the NICMOS focus has been seen since the beginning of operations (Suchkov 1998; Suchkov & Hershey 1998; Storrs & Hershey 1998). It modulates the optical path length of the HST telescope assembly and is caused by the varying thermal environment as the telescope orbits from night to day. The effect also depends on the orientation of the telescope during the orbital period. The breathing model described above was used to correct the actual PAM settings during the focus monitoring in the period 1998–1999.

Since the effect is relatively small in PAM space, at most a few tenths of a millimeter, the breathing correction was discontinued following the installation of the NCS in 2002. However, in order to improve the NICMOS focus measurements and determine why the focus seems to have been approximately constant while the location of the HST secondary mirror has changed, we decided to implement breathing corrections following the switch to using encircled energy instead of phase retrieval in the regular focus monitoring program.

NICMOS focus is routinely monitored every two months for NIC1 and NIC2 and every six months for NIC3. The optimal PAM position is determined from a series of 17 exposures, both in and out of focus of a crowded star field taken at several PAM (Pupil Alignment Mechanism) settings covering the full range of its motion (± 10 mm from its zero position). The total number of counts in a fixed aperture is measured for each star at each point in the focus sweep. The PAM position corresponding to the maximum count rate is the best focus. A fit through 8 points near the best focus finds the location of peak energy in PAM

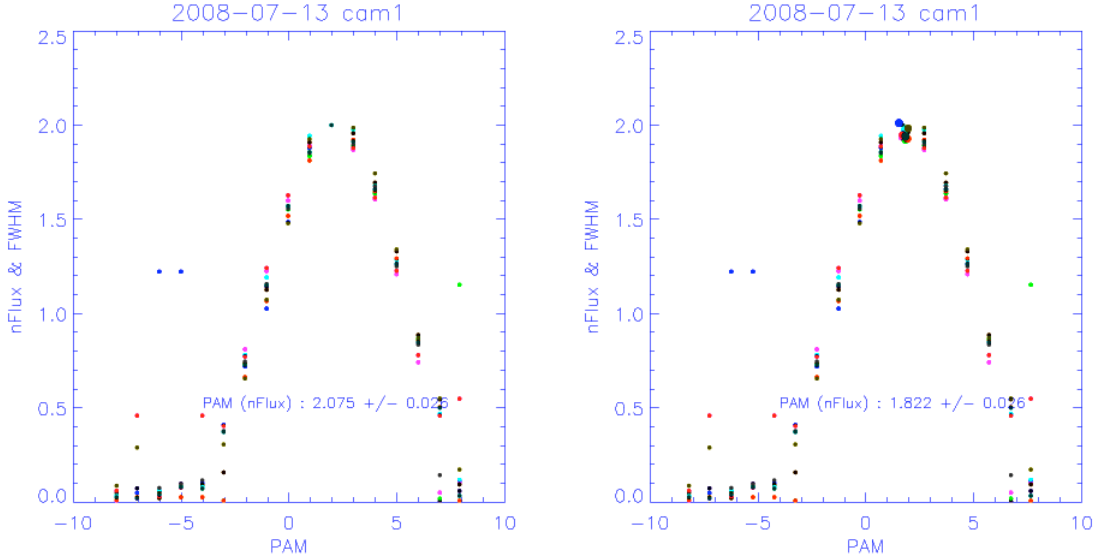


Fig. 3.— *Results from the regular focus monitoring for NIC1. Left: Optimal PAM position measured by routine focus monitoring analysis: $PAM = 2.08 \pm 0.02$. Right: Optimal PAM position including breathing corrections: $PAM = 1.82 \pm 0.03$.*

space as shown in Figure 3.

We use equation 2 to implement breathing correction in regular focus monitoring for NIC1 and NIC2 using the encircled energy method. HST temperature data is collected every five minutes. Figure 2 shows the variation of the light shield temperature over a period of one day. In equation 2, T_{LS4} is the temperature corresponding to each focus exposure and is calculated by interpolating light shield temperatures measured every 5 minutes. The temperature, $\langle T_{LS4} \rangle$, is the light shield temperature averaged over the previous orbit, ~ 90 minutes. The corrected PAM position is then given by:

$$PAM_{\text{new}} = PAM_{\text{old}} + (0.11 \times G_i \times \Delta SM_{\mu\text{m}}) \text{ mm} , \quad (3)$$

where the G_i coefficients for NIC1, NIC2 and NIC3 are given above. This corrected PAM position can be used by regular focus monitoring scripts to calculate the optimal PAM position. This is shown in Figure 3. This analysis also generates files containing the encircled energy at each PAM position (corrected for breathing) for stars in the focus sweep observation. These can be used in the analysis of focus field variation.

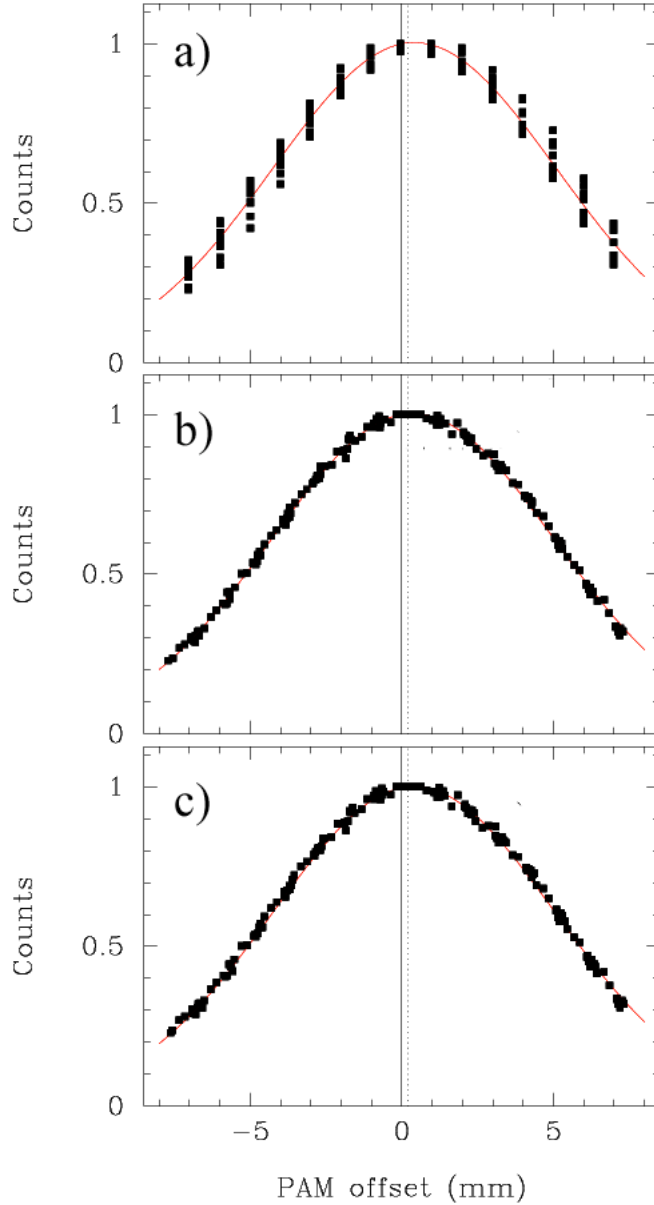


Fig. 4.— **a)** The raw result from a single focus monitoring run with NIC2. The x-axis shows the commanded PAM positions, starting at +7 mm and running to -7 mm in steps of 1 mm. The y-axis shows the normalized encircled energy for 11 different stars spread over the area of the CCD. The red line is the best-fit gaussian. The data is not corrected for breathing, nor focus field variations. The dashed line shows the location of the best-fit PAM position. **b)** Same as a) but correcting for the focus field variation. **c)** Same as b) but also including breathing corrections. In this particular case, the result is essentially indistinguishable from only correcting for focus field variations.

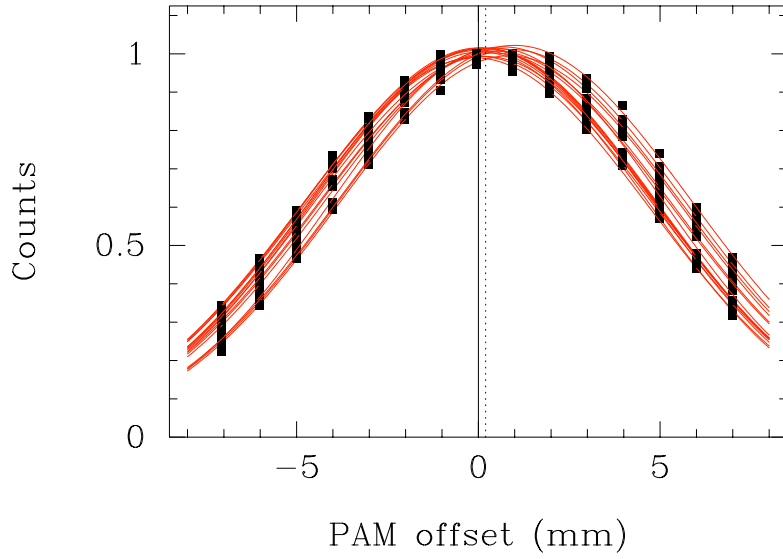


Fig. 5.— *Fits to individual stars for a typical focus monitoring run. The best focus varies depending on the location of a given star on the detector.*

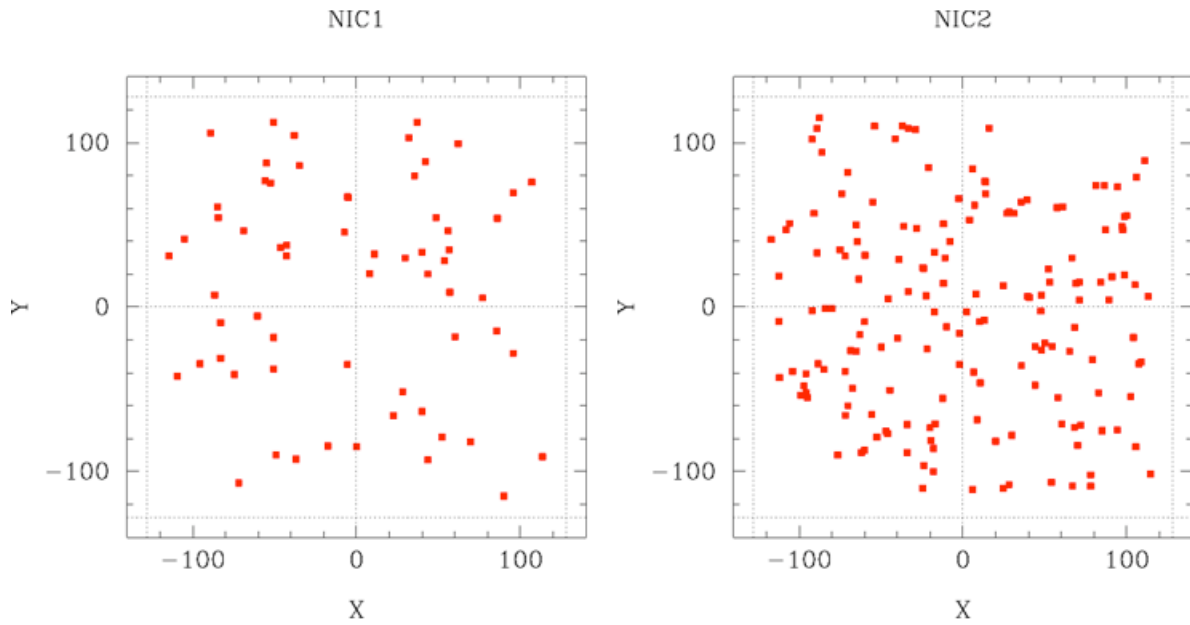


Fig. 6.— *The distribution of stars in the field of view of NIC1 (left) and NIC2 (right) used for defining the second degree surface $g(x, y)$. The number of stars is 63 for NIC1 and 168 for NIC2.*

Focus Field Variations

An effect of the distorted dewar is that the NICMOS cameras are no longer confocal and that the wavefront is not perfectly flat when it meets the NICMOS detectors. Instead the focal plane is curved and the best focus varies over the field of view of the detectors. This effect is quite large for NIC2 and NIC3 in particular, amounting to ~ 1.5 mm in PAM space. The best focus derived from a single star therefore needs to be corrected to a reference pixel. In this case we use the detector center (128,128) as a reference and all focus measurements are corrected to correspond to the focus of this pixel location.

The curvature of the three NICMOS detectors was characterized by Suchkov & Gala (1998). Their results have been used up to this date to compensate for the focus field variations. The characterization of the FFV is prone to uncertainties and the curvature is potentially changing with time. We therefore found it necessary to update the characterization of the curvature of the focal plane for the NICMOS cameras.

Focus Monitoring data used for FFV analysis					
NIC1			NIC2		
Obs date	Target	Prop ID	Obs date	Target	Prop ID
Jan 01 2006	NGC3603	10724	Nov 22 2005	NGC3603	10724
Jun 15 2006	NGC1850	10724	Feb 20 2006	NGC3603	10724
Oct 21 2006	NGC1850	11063	Jun 20 2006	NGC3603	10724
Dec 27 2006	NGC3603	11063	Aug 09 2006	NGC3603	10724
Mar 31 2007	NGC1850	11063	Nov 15 2006	NGC3603	11063
Feb 11 2008	NGC3603	11320	Feb 05 2007	NGC3603	11063
Apr 06 2008	NGC3603	11320	May 11 2007	NGC3603	11063
Jul 13 2008	NGC3603	11320	Feb 10 2008	NGC3603	11320
			May 22 2008	NGC3603	11320
			Aug 12 2008	NGC1850	11320

Table 2: *Dates, target and proposal IDs for the data used in the FFV analysis.*

Data and Analysis

We use a set of data obtained from the regular NICMOS focus monitoring in the period 2006 to 2008 (program ID's: 10724, 11063, 11320) for implementing both the breathing

corrections and for evaluating the curvature of the focal plane. The current focus monitoring program is described in McLaughlin et al. (2007). The focus of the NIC3 camera is only checked twice yearly and we therefore do not have enough data to determine the focus field curvature without using observations extended over a longer time period. Since the NIC3 camera is already out of focus, any FFV effects will have minimal impact on the data quality. We will therefore only analyze the NIC1 and NIC2 cameras.

A focus sweep in the regular focus monitoring program consists of 17 exposures, each with a different setting of the PAM mechanism. This sweep brackets the PAM position corresponding to the best focus. As target we use the outer region of an open cluster (NGC3603 and NGC1805), giving a relatively high stellar density but minimizes the crowding (particularly important as most of the images are highly defocused). A number of isolated stars are selected and the counts within a fix aperture are measured (see McLaughlin et al. 2007). The counts for all the stars are then plotted as a function of PAM position (see Figure 4a) and a gaussian or parabolic function is fitted to the data. The maximum corresponds to the PAM position giving the best focus.

Due to the curvature of the focal plane over the field of view of the detectors, the combined data for several stars will be distributed in a column for each PAM position. This is an effect of the curvature, where the best focus varies from pixel to pixel. This is illustrated in Figure 5, where a separate gaussian fit is made to each individual star of a typical focus monitoring run. As can be seen from the figure, each star has a different best focus position, depending on its location on the detector. If the stars are evenly distributed and the focus curvature is symmetric, the average best-focus should be close to the best focus at the center of the detector. However, due to the limited number of stars available in a given pointing, this is usually not the case and we have no way of ascertaining the precise focus without measuring or compensating for the curvature for each detector.

In principle it is easy to determine the curvature: measure the PAM position corresponding to best focus for each pixel and then reference this to a given pixel position on the detector. In practice, however, the curvature measurement is difficult due to the sparse distribution of stars over the field of view, the uncertainty associated with each measurement and the breathing effects (which effectively adds to the measurement noise).

In Suchkov & Galas (1998) the curvatures for the NICMOS cameras were derived by plotting the PAM positions for best focus as a function of rows and columns separately. A parametrized second degree surface was then fitted to the data. We use a slightly different approach fitting the same type of second degree surface:

$$g(x, y) = a_1 x + a_2 y + a_3 x^2 + a_4 y^2 + a_5 xy, \quad (4)$$

where (x, y) corresponds to a pixel position on the detector. Pixel $(0, 0)$ represents the detector center and hence, with this representation, the center always corresponds to zero curvature. The curve in Figure 4a is well represented by gaussian profile and we will therefore characterize the focus data as

$$f(z) = a_0 \exp\left(-\frac{[z + g(x, y)] - z_0}{w}\right)^2, \quad (5)$$

where z_0 is the PAM position for best focus at $(x, y) = (0, 0)$ (e.g. the detector center), w and a_0 are the width and amplitude of the gaussian function, respectively. The term $g(x, y)$ represents the second degree surface as a function of pixel position (x, y) . The PAM position in millimeter is given by z and the function $f(z)$ corresponds to the normalized encircled energy.

In total there are 8 parameters; 5 parameters describing the second degree surface and 3 parameters describing the shape of the gaussian profile (amplitude, width and location). There are $17 \times N$ variables, where N is the number of stars used in the fitting process, typically 15–20. In order to improve the errors, we only use 10–11 of the 17 PAM positions in the fit. We minimize the function $f(z)$ using a Levenberg–Marquardt algorithm. The resulting fit is shown in Figure 4b. In this particular case the scatter is very small and the PAM position for best focus is well determined. In Figure 4c we do the same fit but now also correcting for breathing. The result is essentially identical to the case without breathing corrections. In general, the goodness-of-fit improves when including the breathing correction.

A single focus sweep does not provide enough stars to determine the function $g(x, y)$ with a high degree of confidence. This is seen as a relatively large dispersion in the parameter values a_1, \dots, a_5 for different focus sweeps, even if the individual χ^2 values are acceptable. This is caused by an uneven distribution of stars across the field of view in a given focus run. We therefore combined all the data from the focus monitoring runs listed in Table 2 in the fitting procedure. This produces a more even distribution of measurement points over the detector field of view (see Figure 6). The number of stars in NIC1 is 63 while we have 168 stars in NIC2. This is simply an effect of the smaller field of view of NIC1. We also experimented with keeping the gaussian parameters fixed, including the PAM position for best focus, z_0 . However, fitting all 8 parameters does give a nominal PAM position

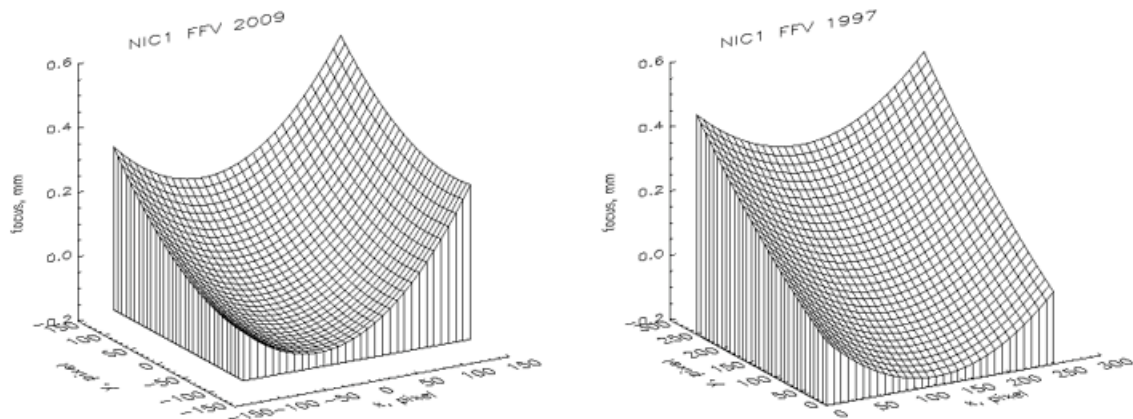


Fig. 7.— *NICMOS Focus Field Variation for NIC1 as given by equation 5 and with coefficients from Table 3. The figure on the left is plotted using the new results and the figure on the right shows the result from Suchkov & Galas (1998).*

very similar to the average for all post-SM3b focus monitoring results (Figure 1) of 2.0 mm and 0.4 mm for NIC1 and NIC2, respectively. The coefficients, a_1, \dots, a_8 , characterizing the curvature do not show a strong dependence on the number of parameters used in the fit (that is, 5 or 8). The adopted parameters characterizing the curvature for NIC1 and NIC2 are listed in Table 3 and the shape of the surfaces are shown in Figure 7 and 8. As can be seen the new curvature differs slightly from the ones determined in 1997. The difference is at a level of ~ 0.1 mm in PAM space. This small difference is not significant given the uncertainty associated with the determination of the coefficients.

Conclusions and Summary

The results presented here show that correcting for the orbital variation in the HST focus, so called breathing, improves the determination of the NICMOS PAM position corresponding to optimal focus. The improvement corresponds to a few tenths of a millimeter in PAM space.

A new determination of the NICMOS focus field variation, using a different technique from the one previously applied, shows that the curvature of the focal plane over NIC1 and NIC2 has remained approximately constant since 1998. Small variations on the order of 0.1 mm in PAM space cannot be excluded with the present data and analysis.

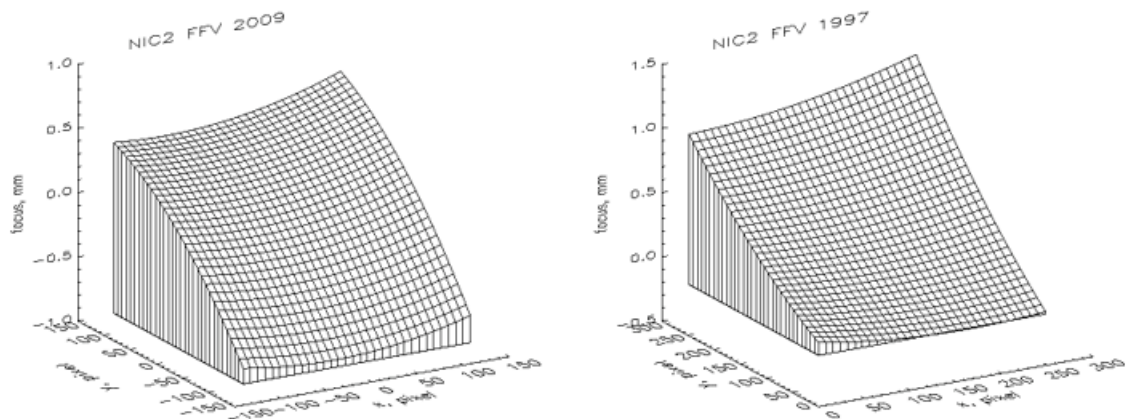


Fig. 8.— Same as Figure 7 but for NIC2. The figure on the left shows our new results and the right hand figure shows the result from Suchkov & Galas (1998).

Camera	$a_x \times 10^3$	$a_y \times 10^3$	$a_{xx} \times 10^5$	$a_{yy} \times 10^5$	$a_{xy} \times 10^5$
NIC1	1.225 ± 0.877	1.224 ± 0.549	1.584 ± 0.501	0.538 ± 0.331	-0.180 ± 0.432
NIC2	0.715 ± 0.103	5.072 ± 0.218	0.683 ± 0.034	-1.143 ± 0.018	0.234 ± 0.026
NIC3	-3.682 ± 0.159	-6.578 ± 0.120	1.580 ± 0.0166	1.710 ± 0.039	-0.055 ± 0.062

Table 3: Coefficients of the FFV fit from this analysis. Note that the NIC3 values are the same as in Table 1.

The best focus for NIC1 and NIC2 are found to be 2.0 ± 0.1 mm and 0.4 ± 0.2 mm, respectively. These values are similar to the nominal PAM positions in use. It thus seems that the NICMOS focus has not changed significantly over the course of seven years. However, the monotonic change of the position of the secondary mirror, which has been compensated for by three readjustment of the SM position is not detected in the NICMOS focus data. This may indicate that the intrinsic variation of the NICMOS focus is not characterized well enough to detect such small focus variations.

The new breathing corrections and focus field variations will be implemented in the regular NICMOS focus monitoring program for Cycle 17 and later epochs.

Acknowledgments

We would like to thank Matt Lallo for illuminating discussions and clarifications and Pey-Lian Lim for valuable insights and tips on IDL programming.

References

- Di Nino, D., Makidon, R.B., Lallo, M., Sahu, K.C., Sirianni, M. & Casertano, S. 2008, ACS ISR 2008-003
- McLaughlin, H., & Wiklind, T. 2007, NICMOS ISR 2007-003
- Storrs, A.D. & Hershey, J.L. 1998, NICMOS ISR 98-009
- Suchkov, A. 1998, NICMOS ISR-98-007
- Suchkov, A. & Galas, G. 1998, NICMOS ISR-98-005
- Suchkov, A. & Hershey, J. 1998, NICMOS ISR 98-015